ＩＳＳＮ１３４６－７８３２

独立行政法人港湾空港技術研究所

港湾空港技術研究所報告

REPORT OF THE PORT AND AIRPORT RESEARCH INSTITUTE

VOL.46 NO.2 June 2007

NAGASE, YOKOSUKA, JAPAN

INDEPENDENT ADMINISTRATIVE INSTITUTION,
PORT AND AIRPORT RESEARCH INSTITUTE

港湾空港技術研究所報告（REPORT OF PARI）
第 46 巻　第 2 号（Vol. 46，No. 2），2007 年 6 月（June 2007）

目　　次（CONTENTS）

REPORT OF THE PORT AND
AIRPORT RESEARCH INSTITUTE
Vol.46, No. 2 (June. 2007)

Cracking and Tension Stiffening Behavior of Corroded RC Members

Jianguo DAI*
Ema KATO*
Mitsuyasu IWANAMI*
Hiroshi YOKOTA**

Synopsis

This paper studied experimentally and analytically the tension stiffening and cracking behavior of corroded uni-axial RC members. Eighteen RC members of 2.0m in length were prepared for the experimental tests and thirteen of them had experienced different levels of impressed current deterioration. Test variables included rebar type, rebar diameter, and transverse confinement condition. The steel corrosion and cracking distributing properties, corrosion-induced bond loss, and the corrosion-induced tension stiffening deterioration were investigated in details. It was found through the tests that the localized deformations, namely the corrosion-induced cracks and it-affected loading cracks, are highly correlated with the un-uniformity of steel corrosion. Moreover, it was concluded that, compared to the losses of steel cross-section and effective concrete cover, the bond loss-induced tension stiffening deterioration may be not a critical factor responsible for the global stiffness loss of corroded RC members.

Further careful analysis based on a discrete modeling approach was performed to quantitatively clarify the relationship between the tension stiffening deterioration and the corrosion-induced bond loss. It was understood through the analysis that the corrosion-induced bond loss may not cause severe tension stiffening loss except when the steel corrosion is extremely severe. The reason is that the tension stiffening reflects the coupled effects of many factors like the crack spacing, corrosion-induced reinforcement ratio loss, and the bond deterioration. This analytical finding coincided well with the experimental one. On the other hand, analysis also showed visually that the increase of the localized crack width induced by the steel corrosion should be a major concern for the structural performance deterioration of the corroded RC members related to the serviceability.

This research provides information useful for the appropriate evaluation of the remained serviceability of corrosion-deteriorated RC structures in practice.

Key Words: reinforced concrete, corrosion, cracking, bond, tension stiffening, un-uniformity of steel corrosion

* Project Researcher, Life Cycle Management(LCM) Research Center for Coastal Infrastructures
** Director General, Life Cycle Management(LCM) Research Center for Coastal Infrastructures
3-1-1 Nagase, Yokosuka, 239-0826 Japan
Phone : +81-46-844-5089 Fax : +81-46-844-0255 e-mail:dai@pari.go.jp

港湾空港技術研究所報告
第 46 巻第 2 号(2007. 6)

鉄筋が腐食したRC部材のひび割れ性状とテンションスティフニング効果

戴　建国*・加藤　絵万*・岩波　光保*・横田　弘**

要　旨

本研究は，鉄筋腐食によりもたらされる鉄筋コンクリート（RC）部材の構造性能の低下を精緻に評価する手法を確立するための研究の一環として，鉄筋腐食により生じる鉄筋－コンクリート間の付着劣化が RC 部材のテンションスティフニング効果，および RC 部材のひび割れ性状に及ぼす影響について検討を行ったものである．

鉄筋形状，鉄筋径，拘束筋の有無および電食により鉄筋の腐食程度を変化させた RC 部材の一軸引張試験を行い，これらの要因が鉄筋－コンクリート間の付着劣化に及ぼす影響を実験的に把握した．その結果，RC 部材中の腐食発生の不均一性が，腐食ひび割れの発生や載荷時のひび割れ分散性，ひいては載荷時に生じる変形の局所化に大きく影響することが分かった．また，鉄筋とコンクリート間の付着劣化がもたらすテンションスティフニング効果の低下は，腐食による鉄筋の断面減少や腐食ひび割れの発生による有効かぶりの減少と比較して，RC 部材全体の引張剛性の損失に及ぼす影響は小さいことが推測された．

以上の実験結果をもとに，鉄筋腐食がもたらす鉄筋－コンクリート間の付着劣化とテンションスティフニング効果の関係について，離散ひび割れモデルを用いた解析により定量的評価を試みた．解析結果から，RC 部材のテンションスティフニング効果は，鉄筋腐食がもたらす鉄筋－コンクリート間の付着劣化だけでなく，腐食による鉄筋断面積の減少や載荷時のひび割れ発生間隔等，複数の要因に影響されることが分かった．このため，RC 部材中に著しい鉄筋腐食が生じた場合を除いて，鉄筋腐食がもたらす付着劣化はテンションスティフニング効果の損失を招く主要因とはならないことが考えられた．さらに，鉄筋腐食が生じた RC 部材では，載荷により生じるひび割れの分散性が低下し，ひび割れ幅が局所的に増加することにより，部材の構造性能が低下することが明らかとなった．

キーワード：鉄筋コンクリート，鉄筋腐食，ひび割れ，付着，テンションスティフニング効果，鉄筋腐食の不均一性

* LCM研究センター　特任研究官
** LCM研究センター長
〒239-0826　横須賀市長瀬3-1-1　独立行政法人港湾空港技術研究所
電話：046-844-5089　Fax：046-844-0255　　e-mail:dai@pari.go.jp

Contents

1. Introduction

Corrosion of steel reinforcement due to chloride attack is a severe problem for the port reinforced concrete (RC) structures. It leads to cracking of concrete, reduction of steel cross-section, loss of bond strength between steel reinforcement and concrete, and eventually loss of structural safety. Unfortunately, in practice the time to corrosion initiation in port RC structures proves to be short compared to their expected service life. Therefore, it has a great necessity to evaluate the current and to predict the future structural performance deterioration of corroded RC structures in order to formulate optimized life cycle management strategies. Generally, two major topics are addressed for these corrosion-deteriorated RC structures. One is to study their remained safety in terms of the residual strength and ductility, in which cases the loss of steel cross-section and the change of failure mechanisms may be primary concerns. Another is to study their remained serviceability in terms of the cracking propagation and stiffness degradation, which are main focuses for discussion in this paper.

Tension stiffening of concrete after cracking is one of the most important factors that influence the performance of RC members concerning the serviceability. Extensive tests and theoretical modeling have been conducted to investigate the relationship between the steel corrosion level and the bond strength loss between the steel reinforcement and concrete (Auyeung et al. 2000; Coronelli 2002; Lee et al. 2002; Fang et al. 2004; JCI Report 2004; Lungren et al. 2005a, 2005b; Aramasa 2005; Amleh and Ghosh 2006; JSCE Report 2006). However, it is noticed that only limited databases on the corrosion-induced tension stiffening deterioration are available up to now (Amleh and Mirza 1999; Matsuo et al. 2001; Kato et al. 2003). In the meantime, the quantitative relationships among the corrosion-induced bond loss, the average tension stiffening deterioration, and the global stiffness degradation remain un-clarified.

Crack width is another serviceability-related concern for RC members. A lot of models have been developed to predict the corrosion-induced crack widths. Moreover, experimental studies have also been performed to study the crack dispersing properties in corroded RC members under mechanical loading (Kato et al. 2003, 2006). However, attention shall be paid to that the corrosion-induced or affected cracks are involved in large scatters that are caused by many uncertainties such as the un-uniformity of steel corrosion. When the crack width is used as an index for serviceability evaluation or an input for predicting the further deterioration of the structural performance of corroded RC members, it has obvious necessity to understand its distributing characteristics from a more localized point of view while considering the un-uniformity of steel corrosion. In the past, only few investigations focused on this aspect (Okazaki et al. 2003).

Regarding this background, a test program for a series of un-corroded and corroded RC tensile members was performed in this paper with focuses on the following two topics: (1) to study corrosion-induced crack widths and it-affected crack widths under external mechanical loading by correlating them to the un-uniformity of steel corrosion; and (2) to study corrosion-induced bond loss and the way by which it influences the global tension stiffness. In addition, the paper also performed careful analysis based on a discrete modeling approach to reproduce the cracking distributing behavior of un-corroded and corroded RC members subjected to uni-axial loading, also to simulate the tension stiffening behavior of cracked concrete, which plays a bridging role in linking the corrosion-induced bond loss to the global member stiffness degradation of corroded RC members.

2. Experimental Program

2.1 Experimental Materials and Specimens

Eighteen uni-axial RC members with a 150×200mm rectangular section and 2.0m in length were prepared for tests (see **Fig.1**) Test variables included steel reinforcement type (D19-1, D19-2 and D25), transverse confinement ratio (none, D6@150mm, and D6@75mm), and steel corrosion level (the actual average steel mass loss varied from 0.0% to 12.3%). The used concrete had a compressive strength of about 40 MPa at the age of testing. **Tables 1** and **2** present the mixing proportion of concrete and the mechanical properties of all used steel reinforcement, respectively. The steel D19-1 was

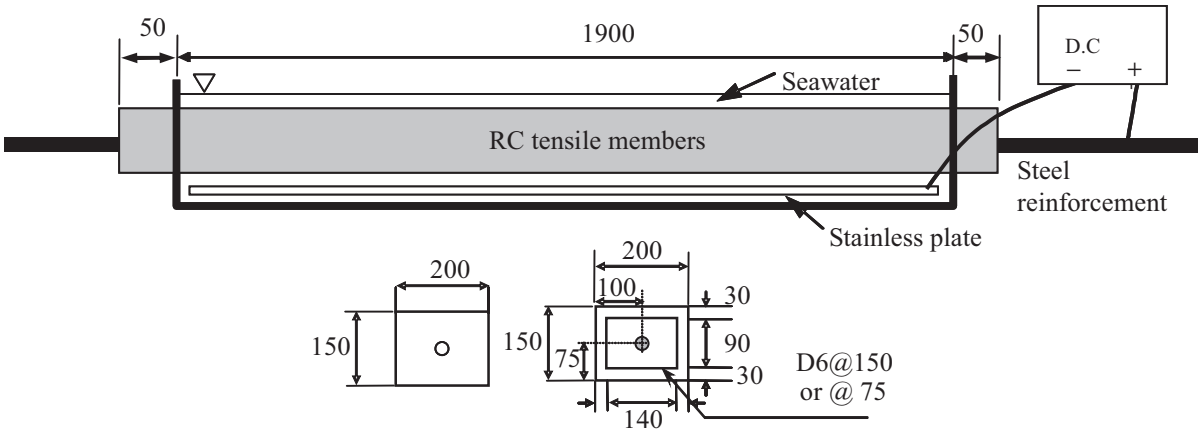

a) without confinement b) with confinement unit: mm

Fig.1 Dimension of Specimens and Impressed Current Deterioration

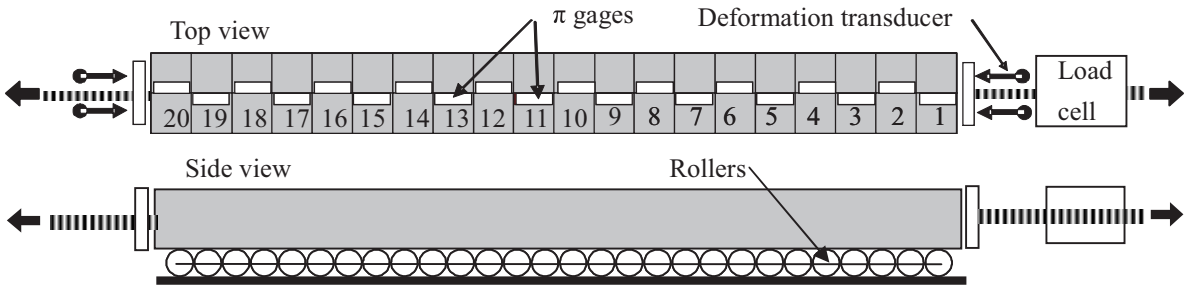

Fig.2 Loading System

screwed deformed (NEJI TEKKON) type while the remained were normal deformed type. The ribs of screwed and normal deformed bars were diagonal and vertical, respectively, to their axis and the height of ribs in the screwed deformed bar was comparatively large. Summaries of all the specimens are provided in **Table 3.**

Table 1 Mixing Proportion of Concrete

G_{max} (mm)	W/C (%)	s/a	Amount (kg/m^3)				
			W	C	S	G	AE
20	56.5	0.43	160	284	790	1080	0.568

Note: G_{max} =maximum size of coarse aggregates; W = water; C = cement; S = sand; G = gravel; s/a = sand to gravel ratio; and AE=air-entraining admixture additive.

Table 2 Properties of Steel Reinforcement

Type	E_s (kN/mm^2)	f_y (N/mm^2)	f_u (N/mm^2)
D19-1	190	362	418
D19-2	206	378	539
D25	206	388	542
D6	-	401	474

Note: E_s =Young's modulus; f_y =yielding strength; and f_u = fracture strength.

Table 3 Summary of All the Tested Specimens

Code	f_c' (MPa)	Steel reinforcement		C_s (%)
		Longitudinal	Transverse	
T1-1	39.3	D19-1	None	0.00
T1-2				0.66
T1-3				2.85
T1-4				2.48
T1-5				5.55
T1-6				10.60
T1-C1-1	40.7		D6@ 150mm	0.00
T1-C1-2				12.26
T1-C2-1			D6@ 75mm	0.00
T1-C2-2				10.89
T2-1	39.6	D19-2	None	0.00
T2-2				1.79
T2-3				2.84
T2-4				10.83
T3-1		D25	None	0.00
T3-2				1.14
T3-3				2.17
T3-4				10.92

Note: f_c' = compressive strength of concrete; and C_s = mean steel mass loss.

2.2 Impressed Current Deterioration

Among the tested eighteen RC members thirteen were

introduced corrosion using impressed current method (see **Fig. 1**). Each of them was accelerately deteriorated to a certain corrosion level, which was controlled by monitoring the corrosion-induced crack width at the surface of concrete. It should be mentioned that two end parts 50 mm in length of each specimen remained un-corroded for the purpose of performing loading test as shown in **Fig. 1**. After finishing the corrosion-introducing process, the crack widths on the concrete surface were carefully read along the longitudinal dimension of corroded RC members with a comparatively small interval of 100 mm, so that the distributing properties of steel corrosion could be evaluated.

2.3 Loading System

A load-controlled test system shown in **Fig. 2** was applied to perform the uni-axial tensile tests for all un-corroded and corroded RC members. During the experiments, the load and corresponding tensile deformation within the testing span (2.0 m) of each specimen were recorded. Also, an array of transducers (π gages) were attached on the surface of each tested specimens to trace the occurrence and propagation of tensile loading cracks. Concerning the interval applied for observing steel corrosion, the gage length for all the transducers was also taken as 100 mm.

2.4 Evaluation of Steel Corrosion

After loading tests, all the tested specimens were demolished and then the steel reinforcement was removed from the concrete and cut into many small pieces 100 mm in length. After that these small pieces were measured their mass losses after the surface treatment with sandblasting and 10% diammonium hydrogen citrate solution. Since the same short length 100 mm was applied for the evaluation of corrosion levels (steel mass losses), corrosion-induced cracks, and the cracks in the RC members under mechanical loading, it was possible to investigate their distributing characteristics along the specimen dimensions as well as to see the correlations between the steel mass loss and the corrosion-induced crack width and it-affected loading crack width from a viewpoint of localization of the steel corrosion.

3. Test Results and Discussion

3.1 Un-uniformity of the Steel Corrosion

The un-uniformity of steel corrosion is a typical characteristic of corroded RC members and also an important input for the analysis of both stiffness and strength deterioration. **Figure 3** presents the experimentally obtained distribution of steel corrosion in terms of the local steel mass loss for all thirteen corroded RC members. Data of eighteen steel segments from each specimen are included (data for two segments at the ends of each specimen were removed) and the detailed datasheets can be found in **Appendix I**. All the corroded RC members show significant variations in their local steel mass losses over their whole testing spans. In addition, the normal distribution function seems appropriate to describe this un-uniformity as shown in **Fig. 4**. A larger average steel mass loss, in other words, more severe corrosion usually is accompanied with a greater standard deviation ($S.D$) but a smaller coefficient of variation ($C.O.V$) and vice versa (see **Fig. 4**). This observation is similar to that reported for natural corrosion case (Kato et al. 2006). **Figure 5** compares the un-uniformity of steel corrosion introduced in the laboratory condition and that observed in the natural condition. It is indicated that the $C.O.V$ of the remained steel section increases with the average steel mass loss in both cases, implying that the statistical distributing properties in artificial and natural corrosions are approximately similar. However, the un-uniformity in natural corrosion case is about 1.7 times of that in the artificial corrosion case based on the current database.

3.2 Corrosion-Induced Cracks

During the impressed current deterioration process, a main longitudinal corrosion crack was usually observed at one of the four sides of each corroded specimen. After the corrosion-introducing process and before the uni-axial tensile test, these corrosion-induced crack widths at the concrete surface were carefully recorded (see the datasheets in **Appendix II**). Taking T3 series as an example, **Fig. 6** shows the distribution of the corrosion-induced crack widths at the concrete surface in comparison with that of steel mass losses. It is seen that the peaks of localized steel mass loss and the surface

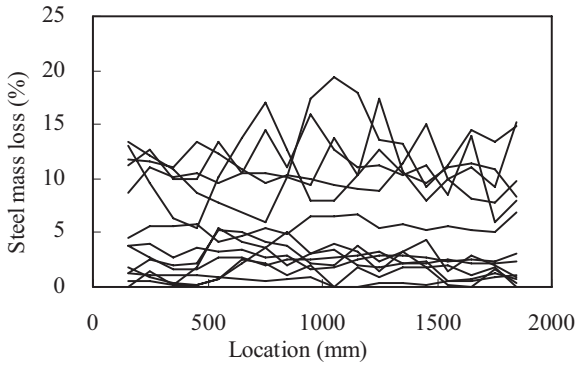

Fig. 3 Un-uniformity of Steel Corrosion

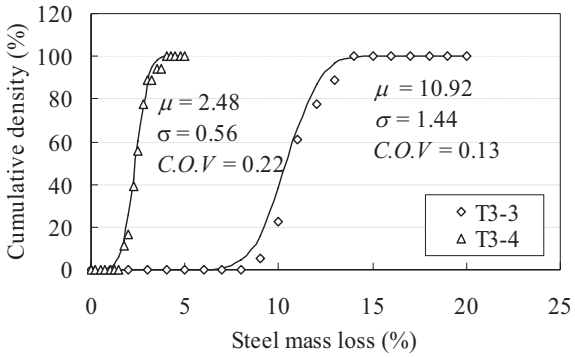

Fig. 4 Normal Distribution of Steel Mass Loss

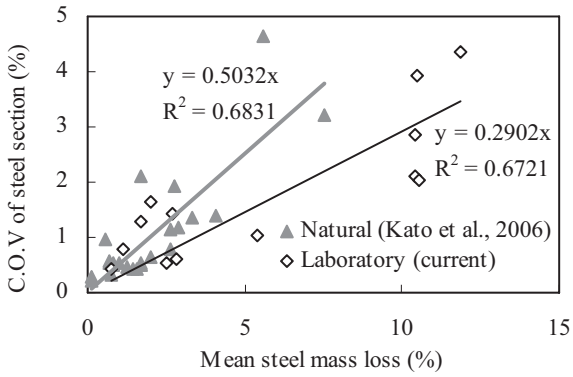

Fig . 5 Comparison of Laboratory and Natural Corrosion

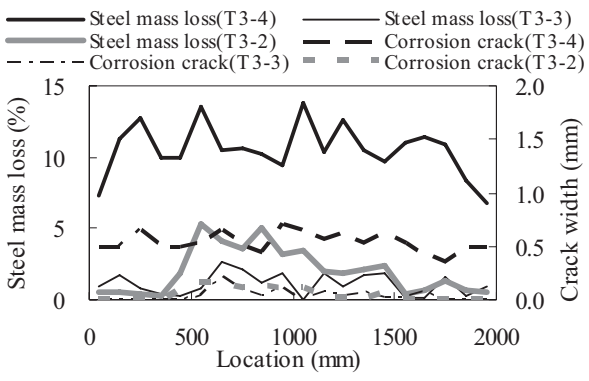

Fig. 6 Distribution of Corrosion-Induced Crack Widths

corrosion cracks coincide well with each other along the longitudinal dimension of the tested members. That is the reason why many researchers have treated the corrosion-induced crack width at the concrete surface as an index of corrosion level in corroded RC members. As a result, numerous models have been developed to predict the relationship between the corrosion crack width and the mass loss of corroded reinforcement (JCI Report 2004). Most of existing models show that the propagation of corrosion follows a behavior like **Eq. (1)**:

$$\Delta w = \gamma \Delta d_s \tag{1}$$

where Δw = the increment of corrosion crack width; Δd_s = the loss of reinforcement diameter; and γ = a constant related to the reinforcement diameter, concrete cover thickness, and the type of corrosion products. A simple solution for γ is to assume that increase in the volume of concrete cracks equals the volume of the corrosion products produced when the diameter of rebar is decreased by Δd_s. As a result, the following expression can be obtained:

$$(\frac{d_s/2}{d_s/2+c_c}+1)c\Delta w = (\alpha-1)\pi d_s \Delta d_s \tag{2}$$

where α = the ratio of the density of the rust product to that of normal steel; and c_c = concrete cover thickness. The diameter loss Δd_s can be expressed by the steel mass loss C_s using the following equation:

$$\Delta d_s = (1-\sqrt{1-C_s})d_s \tag{3}$$

Figure 7 shows the relationship between the localized steel mass loss and the local corrosion crack width that was the summing up of all crack widths at the four sides of each specimen at any locations. The above-mentioned simple assumption seems to be able to describe reasonably the linear relationship between the corrosion crack width and the steel mass loss in spite of the scatter. The values of α are 3.0, 3.9, 2.7 for T1, T2, and T3 test series, respectively, based on linear regression. The different α values in the cases of T1 (D19-1) and T2 (D19-2) series indicate that the rib shape of reinforcement may have an influence on the formulation of corrosion cracks. Also, in case of impressed current method, leakage of rust product from the corrosion cracks may occur. As a result, actual volume of corrosion products to cause expansion may be different

in cases of different rebar diameters since they cause different corrosion crack widths. That is the possible reason for different α values in T2 (D19-2) and T3 (D25) series. Unfortunately, the correlation of corrosion crack width with the steel mass loss seems unclear once the transverse confinement is available (see T1-C series in **Fig. 7**), implying the applicability of the corrosion crack width as a quantitative index to evaluate the steel corrosion is still limited since the confinement conditions in actual corroded RC members are much more complex.

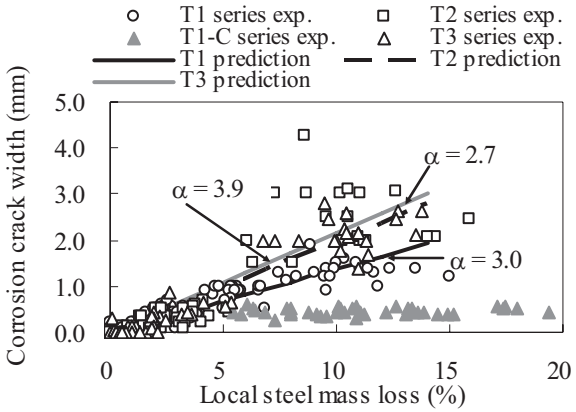

Fig. 7 Relationship between the Steel Mass Loss and the Corrosion-Induced Crack Width

3.3 Distributing Properties of Cracks Formulated under Mechanical Loading

Figure 8 presents the relationship between the steel corrosion level and the maximum crack width, which can be an important index of the remained serviceability. The loading cracks at the same average strain 0.2% of the testing span were chosen for the purpose of comparing all the specimens together. As expected, the crack width increases obviously with the steel corrosion level except when the transverse confinements are available (see **Fig. 8**). The increase is more significant in cases of T1 and T2 series than that in T3 series. In other words, the effect of corrosion on the loading crack width is less significant in cases of high reinforcement ratios. Comparing the testing series T2 to T1, the latter of which had a larger rib height as presented in **Section 2.1**, it is shown that the screwed deformed reinforcement (T1) suppressed the maximum loading cracks in those un-corroded RC members. On the other hand, its crack-bridging ability lost more rapidly

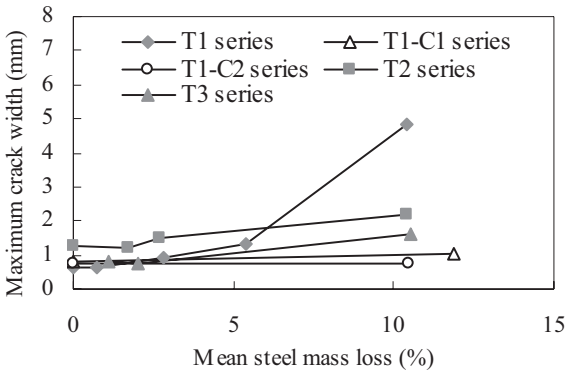

Fig. 8 Influence of Corrosion on Loading Crack Width

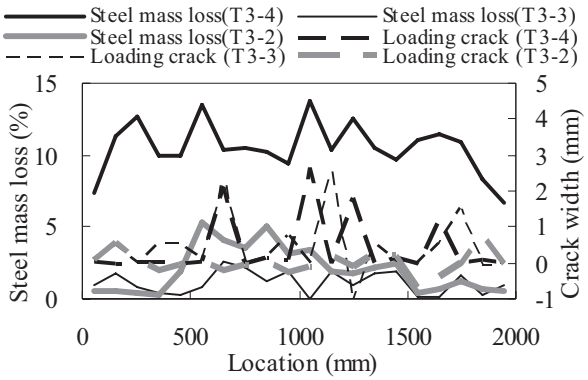

Fig. 9 Comparison of Loading Crack and Steel Corrosion Distributions

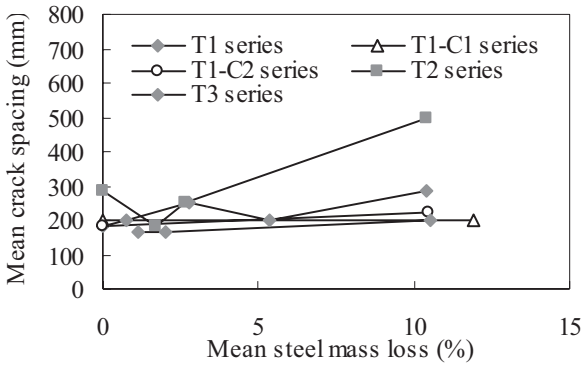

Fig. 10 Effects of Corrosion on Mean Crack Spacing

once a heavy corrosion occurs (see **Fig. 8**). In addition, the peaks of the loading crack widths generally coincide well with those of localized steel mass losses as shown in **Fig. 9**, indicating that these maximum crack widths always occur at the locations where heavier steel mass losses are induced. Therefore, beside the corrosion-induced bond loss, the un-uniformity related to the localization of steel corrosion is considerably a

major factor that influences the loading crack widths in corroded RC members. **Fig. 10** shows the relationship between the steel mass loss and the mean crack spacing. For both T1 and T2 testing series, the reinforcement ratio of which is about 0.96%, the mean crack spacing increases remarkably with the steel mass loss. However, for T3 test series with a reinforcement ratio of 1.65% and a decreased ratio of the concrete cover thickness to steel diameter, this increase is not very significant even though the steel mass loss increases up to 10.53% (see **Fig. 10**). So the effects of corrosion on the crack spacing probably are more remarkable in cases of a low ratio of reinforcement or a large ratio of concrete cover thickness to steel diameter. On the whole, the good correlation among the maximum loading crack widths, crack spacing, and the steel mass loss indicates that localized cracking properties in corroded RC members are strongly related to the un-uniformity of steel corrosion.

3.4 Corrosion-Induced Bond Loss

Change of crack widths and crack spacing in the loaded corroded RC members can be mainly attributed to the corrosion-induced bond loss. If the bond stress distribution between two adjacent cracks is assumed to be uniform, the relationship between the average bond stress and the mean crack spacing can be expressed as follows:

$$\tau = \frac{d_s f_y}{4l} \qquad (4)$$

where τ = the average bond stress between two adjacent cracks; f_y = the yielding strength of rebar; and l = the average crack spacing. **Eq. (4)** shows that the average bond stress is inversely proportional to the average crack spacing. Assuming that τ_0 is the bond strength in cases of un-corroded RC members and using **Eq. (4)**, it is possible to plot the relationship between the residual bond strength τ/τ_0 and the steel mass loss C_s in **Fig. 11**. For all the tested RC members except T2 series, the formulation on corrosion-induced bond loss proposed by JCI–C64 provides a safety margin regardless of the large scatter and provides a best prediction for T1 series. As a result, the JCI-C64 formulation shown in **Fig. 11** is used to simulate the T1 test results in the latter analytical part. However, it is noticed that very few bond losses occurred as the result of corrosion if there was transverse reinforcement available. Hence the steel mass loss may not always be a good parameter to evaluate the bond loss of the interface between the corroded reinforcement and concrete since it may depend more or less on the transverse confinement existing around the main reinforcement in practice. To solve this difficulty, **Fig. 12** plots the relationship between the bond loss and crack width of concrete induced by corrosion putting the confinement and no confinement cases together. It is found that an approximately linear relationship between the corrosion-induced crack width at the concrete surface and the residual bond strength can be obtained. Therefore, the corrosion-induced crack width may provide a better parameter than the steel mass loss through which the residual bond strength can be evaluated. In practice, inspection of the concrete surface cracks may provide good information for the evaluation of the remained bond of the steel reinforcement to concrete although it may not be able to reflect the steel corrosion level correctly as discussed in **Section 3.2**.

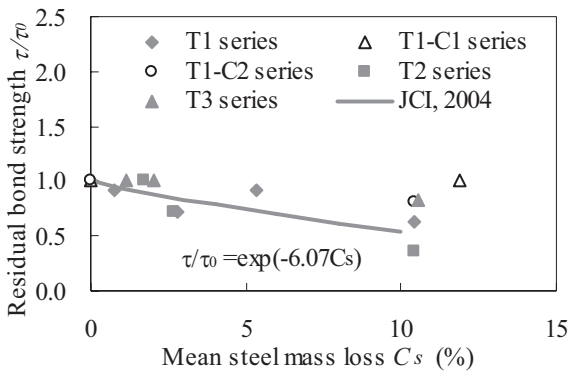

Fig. 11 Influence of Corrosion on the Bond

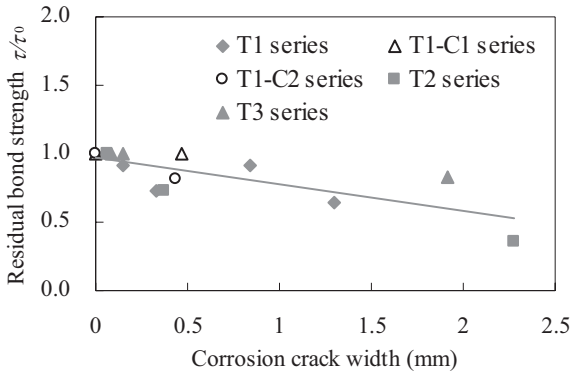

Fig. 12 Influence of Corrosion Crack Width on the Bond

3.5 Corrosion-Induced Tension Stiffening Loss

Taking the T1 (without transverse confinement) and T1-C (with transverse confinement) series for example, **Figs. 13** and **14** show the relationships between the tensile load and the average strain of concrete for these two test series, respectively. Clearly, the load at the same average tensile strain after the concrete cracking decreases with the increase of corrosion level, indicating the deterioration of the global tension stiffness of corroded RC members. This tension stiffness loss is considerably attributed to the following three factors: (1) corrosion-induced reduction of steel cross-section; (2) damage in concrete cover like the corrosion-induced micro or macro-cracks; and (3) corrosion-induced reduction of bond strength between the steel reinforcement and concrete. Theoretically, the relationship between the average tensile strain and the tensile load can be expressed as follows:

$$P = E_s A_s \varepsilon_{aver} + P_{cr}(\frac{\varepsilon_{cr}}{\varepsilon_{aver}})^c \qquad (5.a)$$

$$P_{cr} = f_t A_{c,e} \qquad (5.b)$$

where P = tensile load; E_S = elastic modulus of steel reinforcement; A_s , $A_{c,\,e}$ = effective cross-section of steel reinforcement and concrete, respectively; P_{cr} = tensile load at the first crack of concrete; ε_{cr} = strain of concrete at first cracking; ε_{aver} = average tensile strain of tested specimens; and c = tension stiffening factor taking into account the bond characteristic of steel reinforcement, and usually c = 0.4 for normal deformed bars and larger c means a worse tension stiffening effect. At the right-hand side of **Eq. (5.a)**, the first part reflects the effects of corrosion-induced steel cross-section loss on the global tension stiffness deterioration. The second part reflects the tension stiffening effect contributed by the effective tensile area of concrete between two adjacent concrete through the bond, which is well-known to structural engineers. As shown in **Eq. (5.a),** this tension stiffening part relies on the first cracking load in terms of the tensile strength of concrete and the effective tensile cross section of concrete, and the tension stiffening factor c, which is supposed to be influenced by the corrosion-induced bond loss.

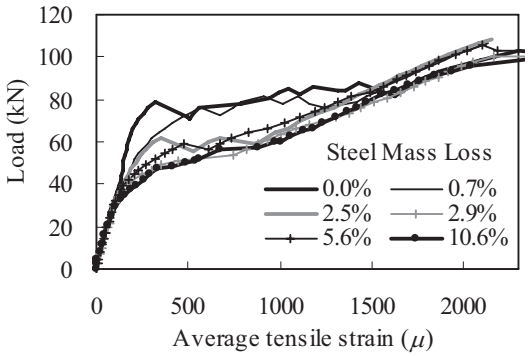

Fig.13 Load-Average Tensile Strain Curves (T1 series)

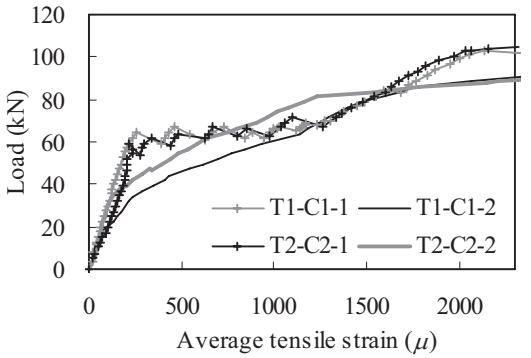

Fig. 14 Load-Average Tensile Strain Curves (T1–C series)

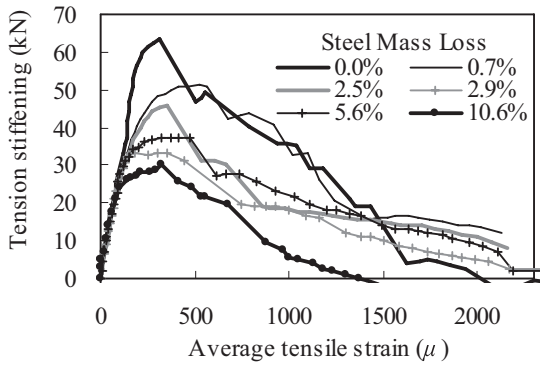

Fig. 15 Corrosion-Induced Tension Stiffening Loss (T1 series)

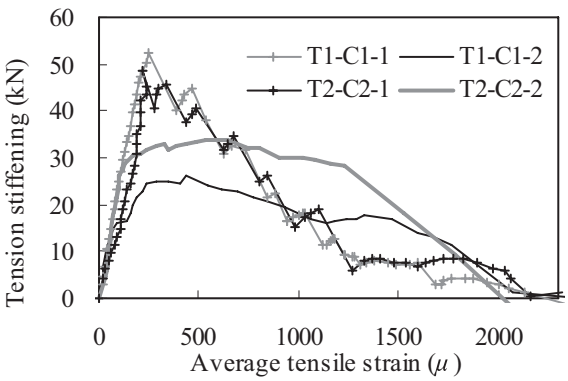

Fig. 16 Corrosion-Affected Tension Stiffening (T1-C series)

Using **Eq. (5)** it is possible to obtain the relationships between the average tensile strain and tension stiffening effects as plotted in **Figs. 15** and **16** for T1 and T1-C series, respectively. The different peaks *Pcr* in these curves indicate that the effective tensile areas of concrete cover are different under different corrosion levels. The possible reason for this is that the steel corrosion induced some irregular crack surfaces in the concrete cover which resulted in the stress uniformity in concrete under the tension loading. When the mechanical behavior of corroded RC members under loading is modeled, this type of non-homogeneity in concrete can be expressed using reduction of effective concrete cover for the simplicity. Otherwise, three dimensional simulations may be required to first reproduce the formulation of corrosion-induced crack surfaces in the concrete cover, and then these preloading damages can be input for further loading analysis. That is beyond the objectives of this study but remains for further research interests. In this paper a simple bi-linear relationship between the reduction factor of effective concrete cover and the mean steel mass loss has been applied based on back-calculation of the test results as shown in **Fig. 17.**

According to **Eq. (5)**, if all the tension stiffening curves shown in **Figs. 15** and **16** are normalized by their peak loads *Pcr,* respectively, the effects of corrosion on the tension stiffening factor can be obtained as plotted in **Fig. 18**. It has to be recognized the difficulty in concluding any clear differences between those un-corroded (solid points) and corroded (void points) RC members in terms of their normalized tension stiffening, or in other words, their tension stiffening factors *c,* within the applied corrosion levels. Qualitatively, it was usually thought that worse bond leads to deteriorated tension stiffening. To interpret well the observed experimental results in **Fig. 18**, it is necessary to know the quantitative relationship between the steel corrosion-induced bond loss and the bond loss-induced tension stiffening, which is an issue to be solved in the analytical part of this paper.

On the whole, the observed tension stiffness loss of corroded RC members can be merely explained in terms of the corrosion-induced steel cross-section reduction and the reduction of effective tensile area of concrete cover. However, within the applied corrosion levels in this test, the steel corrosion seems to have marginal effects on the tension stiffening factor.

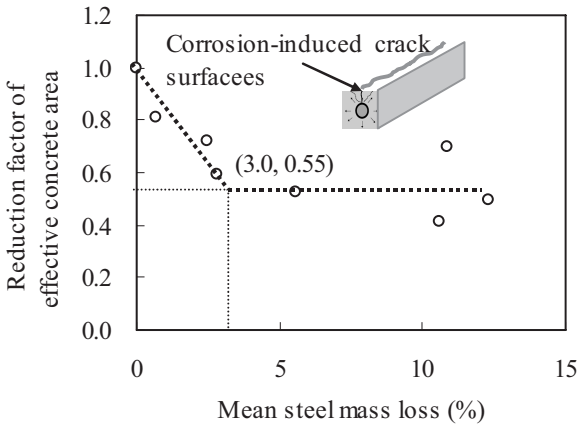

Fig. 17 Corrosion-induced Damage in Concrete Cover

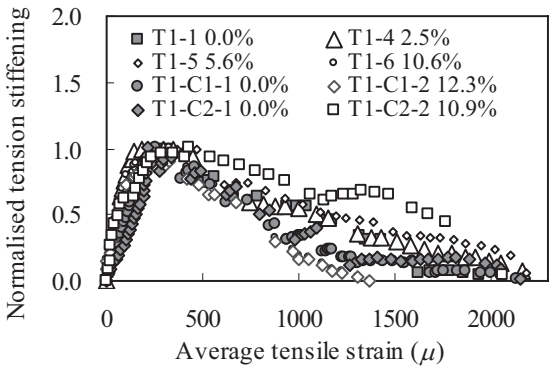

Fig. 18 Relationship between the Normalized Tension Stiffening and the Average Tensile Strain

4. Analytical Programs

To have insightful understanding on the experimental results, careful numerical analysis based on a discrete modeling approach were performed. The main purposes are to reproduce the localized cracking behavior in corroded RC members taking into account the corrosion-induced bond loss, and also, to clarify quantitatively how the corrosion-induced bond loss influences the tension stiffening factor and explain the mechanisms behind the experimental observation. The discrete approach rather than FEA method was chosen because of its strong ability in modeling the discontinuous deformation in concrete like the localized cracks.

4.1 Brief Introduction of the Analytical Tool

The used analytical program was a two-dimensional

one based on rigid body spring network (RBSN) method. RBSN method offers the advantages of describing the discontinuity in material such as cracking, the formulation and distribution of which depends strongly on the bond between steel and concrete. It was first developed by Kawai (1977) and has been extended for analyzing concrete fracture and RC members (Bolander and Saito 1998, 1999; Saito and Hikosaka 1999; Bolander and Le 1999; Nagai et al. 2004, 2005). In this approach concrete are modeled as rigid particles linked with each other through a network of springs at their boundaries. Link elements, which have normal, shear and rotational stiffness, are used between concrete particles and the reinforcement to represent the bond-slip characteristics (see **Fig. 19**). Each concrete particle has three degrees of freedom (*u,v and* θ) at its gravity center. The steel reinforcement is represented as a series of beam elements, each node of which has three degrees of freedom in the axial, shear and rotational directions. To avoid meshing bias, concrete elements are randomly discretized using Voronoi diagrams (Bolander and Le 1999).

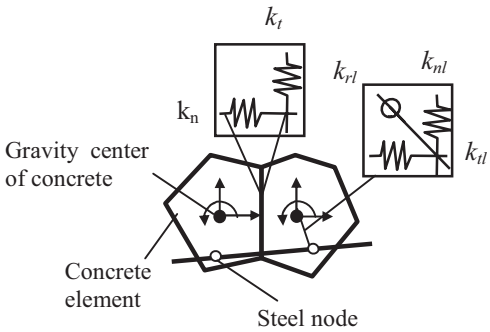

k_n = normal spring stiffness at boundary
k_t = tangential spring stiffness at boundary
k_{nl} = normal spring stiffness of linkage
k_{tl} = tangential spring stiffness of linkage
k_{rl} = rotational spring stiffness of linkage

Fig. 19 Modeling of Concrete and Steel Reinforcement in RBSN Method

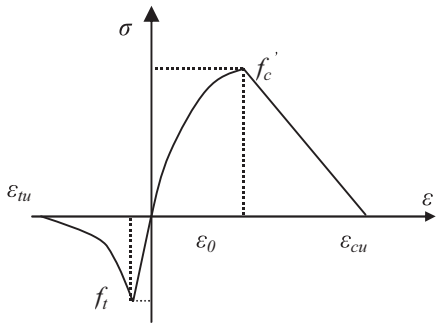

Fig. 20 Constitutive Laws for Normal Spring Connecting Concrete Elements

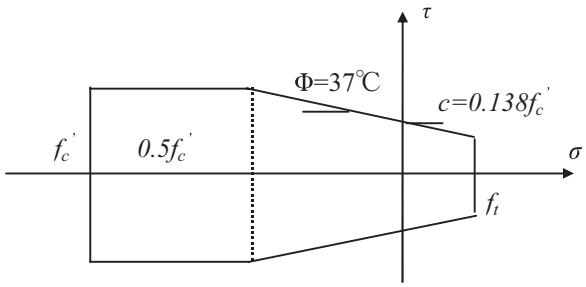

Fig. 21 Constitutive Laws for Shear Springs Connecting Concrete Elements

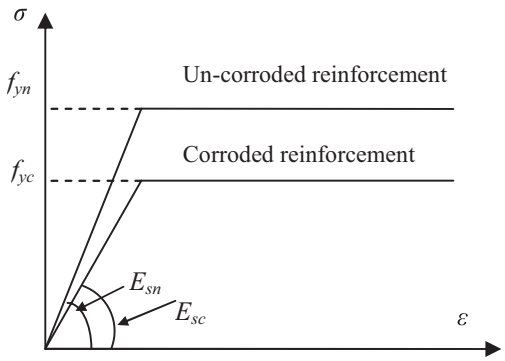

Fig. 22 Mechanical Law of Steel Reinforcement

4.2 Description of Implemented Constitutive Laws

The response of the concrete elements is represented using normal and shear springs of zero size at boundaries between neighboring particles (see **Fig. 20**). The compressive response of the normal springs is given in **Eq. (6.a~c)**.

$$\sigma = \begin{cases} E\varepsilon - E\varepsilon^2/(2\varepsilon_0) \ldots\ldots\ldots\ldots \varepsilon \le \varepsilon_0 \\ f_c' - (\varepsilon - \varepsilon_0) f_c'/(\varepsilon_{cu} - \varepsilon_0) \ldots \varepsilon \succ \varepsilon_0 \end{cases} \quad (6.a)$$

$$\varepsilon_0 = 2f_c'/E_c \quad (6.b)$$

$$\varepsilon_{cu} = 2G_{fc}/(f_c' h) + \varepsilon_0/2 \quad (6.c)$$

where h = the distance between gravity centers of two neighboring particles; and G_{fc} = compressive fracture energy of concrete, which can be taken as $8.8f_c'^{0.5}$ (Nakamura and Higai 1999). Normal spring in tension is assumed to be linear elastic up to concrete's tensile strength f_t , which is calculated using the equation $f_t = 0.23f_c'^{2/3}$ based on JSCE code. The spring stiffness is related to concrete's elastic modulus and Poisson's ratio as defined by Kawai (1977). The tension softening

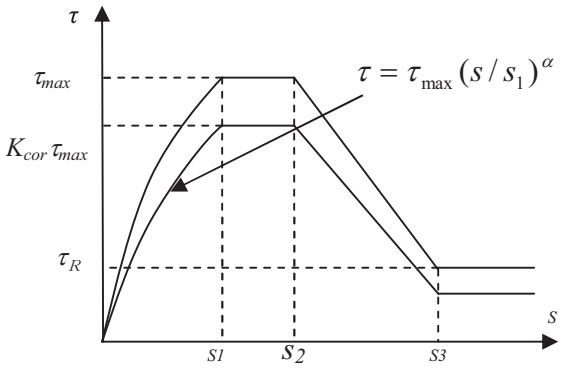

Fig. 23 Bond Stress-Slip Law

model proposed by Reinhardt et al. (1986) was used to describe the behavior of the normal springs after the tensile strength is reached and is given as:

$$\frac{\sigma_f}{f_t} = \{1 + (c_1\delta/\delta_0)^3\}\exp(-c_2\delta/\delta_0) - (\delta/\delta_0)(1 + c_1^3)\exp(-c_2) \quad (7)$$

where $c_1 = 3.0$; $c_2 = 6.93$; and δ = opening displacement between two concrete particles. The maximum opening displacement δ_0, which corresponds to the free tensile stress, is determined based on the **Eq. (8)**, in which fracture energy of concrete is determined by following the CEB-FIP code (1990):

$$\delta_0 = 5.14\frac{G_{ft}}{f_t} \quad (8)$$

The constitutive law developed by Saito and Hikosaka (1999) was applied for the interface shear spring between two concrete particles. In this model, the shear springs of un-cracked interfaces are linear elastic up to the yield surface, which is determined according to the Mohr-Coulomb criterion (as shown in **Fig. 21**). For a cracked interface, an exponential decayed shear softening model was employed after reaching the yield surface and a decreasing factor is introduced to consider the effects of the crack width on the interface shear stiffness and the shear softening. An elastic-perfectly plastic relationship was assumed for the steel (see **Fig. 22**). For the convenience the section of corroded steel is kept constant in the analytical modeling. Instead, the elastic modulus and yielding strength of corroded steel were considered to change with the steel corrosion level as follows:

$$f_{yc} / f_{yn} = 1.00 - K_{fy} \cdot C_s \quad (9)$$

$$E_{sc} / E_{sn} = 1.00 - K_E \cdot C_s \quad (10)$$

where f_{yc}, E_{sc} , and f_{yn} , E_{sn} = the yielding strength and elastic modulus of corroded and healthy steel reinforcement by assuming that there is no change in their cross section in the modeling; C_s = the mass loss of steel in percentage; and K_{fy} was reported to vary between 0.34 and 2.5 while K_E was reported to vary between 0.83~2.3 (JSCE, 2006). In this paper, K_{fy} and K_E are simply taken as 1.0.

Bond between steel reinforcement and concrete is expressed using classical bond-slip expression proposed in CEB-FIP (see **Fig. 23**), where τ_R、α、*S1*、*S2* and *S3* are taken as 0.3, 0.4, 0.05, 0.6 and 1.0, respectively, through fitting the test results. The maximum bond stress τ_{max} is determined using Kemp and Wilhelm (1979)'s model:

$$\tau_{\max} = K_{cor}(0.55 + 0.24\frac{C_c}{d_b}) + 0.191\frac{A_t f_{yt}}{S_s d_b} \quad (11)$$

where C_c/d_b = cover to bar diameter ratio; A_t, f_{yt}, and s_s = the section, yielding strength, and the spacing of transverse reinforcement, respectively; *and* K_{cor} = the bond decay factor due to corrosion and was calculated by the following formulation as has shown in **Fig. 11**:

$$K_{cor} = e^{-6.07C_s} \quad (12)$$

where C_s is corrosion-induced average steel mass loss in percentage.

5. Analytical Results

5.1 Comparison of Cracking Behavior: Experimental and Analytical

Figure 24 shows the meshing information of the analyzed specimens and the obtained crack distributing patterns of RC members after steel reinforcement yielded but at the same average strain level. Several RC specimens without transverse confinement but with typical corrosion levels (steel mass losses) applied for the tests were chosen here for presentation in order to compare more clearly the effects of bond on the crack distributions in the un-corroded and corroded RC members. The crack widths were enlarged 20 times for a

clear view. Similar to the experimental results, the number of cracks (black parts in Fig. 24) formulated during the mechanical loading decreases with the increase of corrosion level in the analysis. On the other hands, the analysis shows visually that the increased mean crack spacing leads to increased crack widths in the corroded RC beams at the same global deformation level (average strain). Those locations, where comparatively dark color is seen, appear reasonably at the mid of two adjacent cracks as theoretically expected, indicating higher tensile stresses in concrete over there. Compared to the experimentally observed crack patterns (see **Fig. 25**), the analysis also gives reasonable prediction for both un-corroded and corroded members in terms of their number of formulated cracks. However, it should be mentioned that the longitudinal corrosion cracks (dotted lines) shown in **Fig. 25** could not be reproduced since the analysis was two-dimensional based and the pre-loading corrosion-induced crack surfaces could not be directly input into the analysis.

Since the maximum corrosion-induced steel mass loss applied in the unconfined RC members was 10.6%, which corresponds to about 50% of original bond according to the **Eq. (11).** Analysis on one more case with a 20% steel mass loss was performed. Analytical results shows that the RC tensile member failed due to the insufficient anchorage length without the occurrence of any cracks over the whole testing span because of the poor interface bond (see the last case in **Fig.24**).

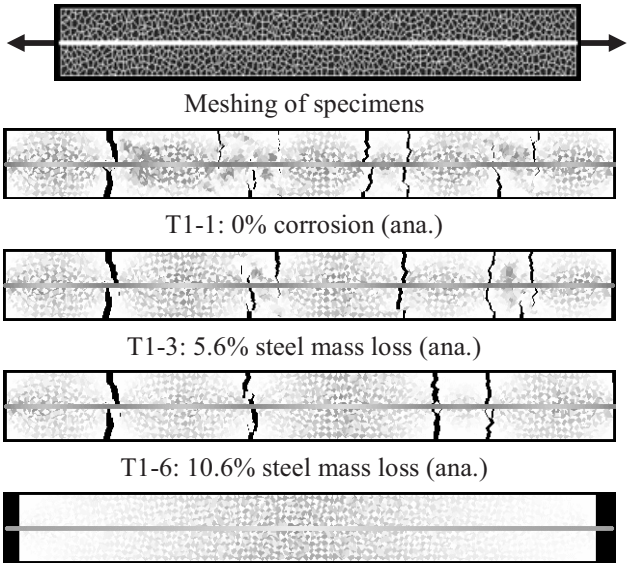

Fig. 24 Crack Distributing Properties Obtained from Analysis

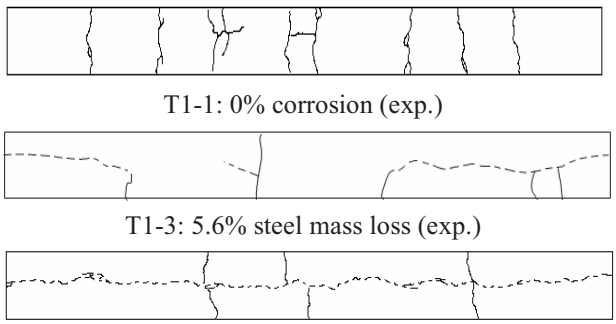

Fig. 25 Crack Distributing Properties Obtained from Experiments

5.2 Comparison of the Global Tension Stiffness: Experimental and Analytical

The experimental and analytical results of the load-average tensile strain responses and the average tensile stress-strain relationships are presented in **Figs. 26** and **27**, respectively. Only three specimens T1-1, T1-3 and T1-6, which represent three different corrosion levels applied in the tests, are presented in these two figures for a clearer comparison. At first, the un-corroded RC member T1 was analyzed. The reasonable agreement between the experimental and analytical results proved the soundness of this analytical program. Then the program was used to analyze the corroded RC members. It was observed in the experiments that the first-cracking tensile loads of the corroded RC members were always much lower than that of un-corroded one. At first the reduction factor of the effective concrete cover as shown in **Fig. 17** was introduced to simulate this deterioration. Since it was not convenient to modify the section area of concrete in the meshing process, as an alternative solution in the analysis, the same reduction factors were introduced to the tensile strength while keeping the effective concrete cross-section constant. As a consequent, if the tension stiffening behavior of cracked concrete is expressed by the average tensile stress-strain curves (see **Fig. 27**) in experiments and analysis, the appeared peaks of these curves are not unique and they are different from the actual tensile strength of concrete. As expected, the analytical load-average tensile strain curves (**Fig. 26)** or

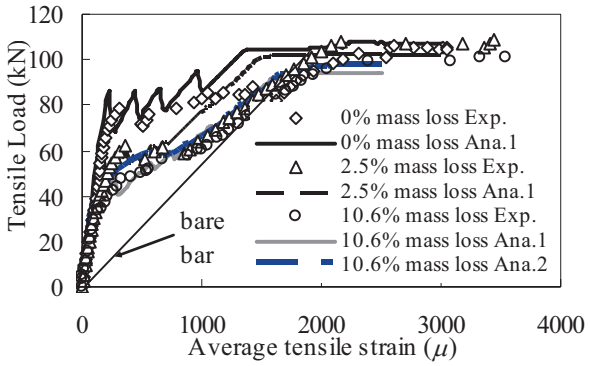

Fig. 26 Experimental and Analytical Tensile Load-Average Strain Responses

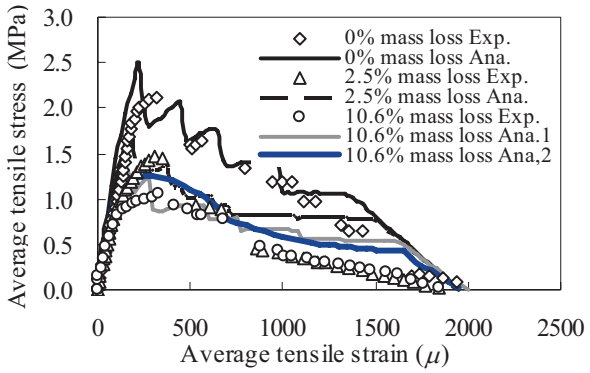

Fig. 27 Experimental and Analytical Tensile Stress-Average Strain Responses

the tension stiffening curves (**Fig. 27**)show acceptable coincidences with the experimental ones (see Ana.1 cases in **Figs. 26** and **27**). However, a remained interest in the analysis after fitting the experimental results was on the issue of whether attributing the tension stiffening deterioration merely to the loss of effective concrete cover rather than the bond loss is true or not. To see whether the bond loss induced by a severe corrosion results in the decrease of the appeared concrete strength in the average tensile stress-strain curves giving a constant effective concrete cover, pair analysis was conducted for the specimen T-6 (10.6 % steel mass loss). It was interestingly found that analytical load-deformation response and average tensile stress-strain curve fit reasonably with the experimental ones if a bond decay factor K_{cor} = 0.90 was introduced in analysis (see Case Ana. 2 in **Figs. 26** and **27**). A further insightful investigation into the failure mode indicated that the corroded RC member with the 90% bond loss would fail in anchorage zone without occurrence of any cracks within the testing span like the T1-X in **Fig. 24**. The reality in the actual tests, however, was that specimens T1-1~6 that had the steel mass losses varying from 0.7% to 10.6% did not encounter any anchorage failure and multi-cracks were observed in these specimens in the experiments as presented in **Fig. 25**. In addition, the bond loss measured indirectly from the tests for the specimen T1-6 was only about 50% as shown in **Fig. 11**. Therefore, the pair analysis verified that to reduce the effective concrete cover was a correct mechanism to explain why the appeared tensile strength of concrete in the average tensile-stress relationship was decreased in the corroded RC members. In the past efforts were mainly focused on studying how the corrosion influences the bond between the steel reinforcement and concrete. However, more efforts may be needed to model the spatial distribution of corrosion–induced initial stress and micro and macro-cracks inside the concrete cover, and also, to quantify their influences on the mechanical behaviors of concrete cover itself from a three dimensional point of view.

On the other hand, the above-mentioned pair analysis for the specimen T1-6 tells that the appeared tensile strength of concrete may be much lower than the actual tensile strength of concrete in the uni-axial tests for the corroded RC members if there are no firm anchorages at the ends of the specimens and if the bond between the reinforcement and concrete is very poor. In other words, the testing boundary conditions applied at the end of corroded tested RC members may affect the calibration of tension stiffening deterioration curves. In order to remove the effects of bond on the appeared tensile strength of concrete in the uni-axial test, strong anchorages that can prohibit the slips between the steel reinforcement and concrete at the ends of specimens may be necessary, so that the obtained first-peak tensile load in the uni-axial tests can reflect more directly the influences of corrosion on the reduction of the effective concrete cover, and in the meantime, the descending parts of the load-deformation curves can reflect directly the effects of bond on the tension stiffening. For un-corroded RC members under the uni-axial tensile tests, the anchorage condition at the ends may be a minor concern because the slip failure between the reinforcement and concrete seldom occurs over there.

5.3 Influences of Bond Loss on the Tension Stiffening Factor: Further Numerical Experimentation

It is commonly known that the tension stiffening model of cracked concrete can be expressed as follows (Okamura and Maekawa, 1990):

$$\sigma_{aver} / f_t = (\varepsilon_{cr} / \varepsilon_{aver})^c \qquad (13)$$

where σ_{aver} = the average tensile stress of cracked concrete; f_t = the actual tensile strength of concrete; ε_{cr} = the tensile strain of concrete at cracking; ε_{aver} = the average tensile strain of concrete; and c = the tension stiffening factor, which is related to not only the bond but also the reinforcing ratio, thickness of concrete cover etc. (Elfgren and Noghabai 2002). The bond is the most influential factor to c. Larger c means poorer bond.

The analysis conducted in the last section verified that the corrosion-induced loss of the effective concrete cover is a major factor responsible for the decrease of the appeared tensile strength of concrete and for the tension stiffening deterioration. A remained un-clarified topic is to explain why the effects of corrosion-induced bond loss on the tensions stiffening deterioration were experimentally marginal within the applied corrosion levels. Concerning the modeling of corrosion-induced tension stiffening deterioration, accurate understanding on the relationship between the corrosion-induced bond loss and the resulting-in tension stiffening loss is required. Therefore, further numerical experimentations for the following two cases were conducted in order to understand how the bond influences the tension stiffening factor in relation to the steel corrosion level:

Case 1: sensitivity analysis of the influence of bond loss (from 10 to 90%) on the c value. The cross section of reinforcement was always kept constant to see the effect of bond loss only on the tension stiffening deterioration. The loading condition was the same as that applied in the current experimental tests.

Case 2: sensitivity analysis of the influence of bond loss (from 10 to 90%) on the c value. The cross section of reinforcement was still kept constant. However, the slips between the reinforcement and concrete at the loaded points were not allowed so that the effects of boundary conditions of anchorage and the possible end anchorage failures in case of poor bond can be removed.

Analytical results for above-mentioned two cases are plotted in **Figs. 28** to **31** in terms of the tensile load versus deformation relationships and the average tensile stress-strain relationships. **Fig. 32** also presents the crack patterns of the specimens used in Case 2 analysis in order to see the effects of testing boundary conditions on cracking patterns. Crack patterns for Case 1 can be referred to **Fig. 24**. Conclusions from these numerical experimentations can be summarized as bellows:

(1) In the specimens without strong anchorages at their ends (Case 1), the first-peak tensile loads (see **Fig. 28**) or the appeared tensile strengths (see **Fig. 29**) show decreasing tendency with the increase of bond loss. When good end anchorages are available, however, the tensile load-average strain response shows a unique peak but usually a sharp decrease after the first cracking depending on bond (see **Fig. 30**). The more the bond loses, the more sharply the tensile load drops after the first peak. The tensile loads versus deformation responses in case of 0% bond loss are almost the same in both cases (see **Figs. 28** and **30**). However, for specimens with the increased bond losses, two different testing conditions lead to significantly different but gradually similar load versus deformation responses at the beginning and latter stages, respectively.

(2) When the bond loss increases from 0 to 90% in Case 1 and Case 2 analysis, the tension stiffening factor c increases from 0.4 to 0.9 and from 0.3 to 0.8, respectively, based on the regression of the analytical average tensile stress-strain relationships shown in **Figs. 29** and **31**. If the changes of tension stiffening factor c with the bond loss in both cases are summarized in **Fig. 33**, in which the corrosion levels corresponding to the given bond losses are also indicated, it can be found that the rates of bond degradation and tension stiffening deterioration are significantly different. In both cases, the tension stiffening factor c just shows a slight increase when the bond loss increases from 0 to 50% (about 10% steel mass loss). After that point the tension stiffening factor c even may change slightly with the corrosion level in an opposite way. Analytically, the 70% bond loss of the original, which corresponds to the steel bond loss of 20%, seems to be a turning point, beyond which the tension stiffening starts to deteriorate rapidly. Of course, in practice a 20% steel mass loss may have led to heavy spalling of concrete cover so that the serviceability

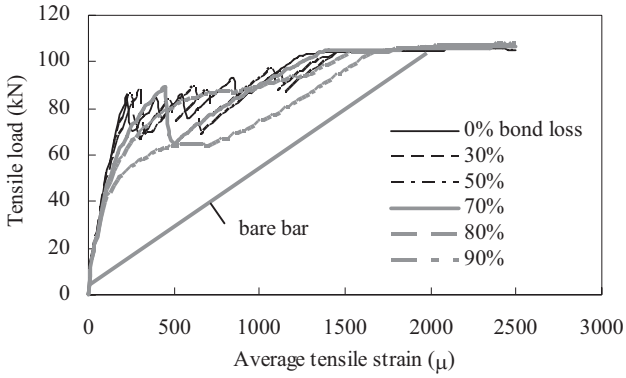

Fig. 28 Tensile Load-Deformation Curves (Case 1)

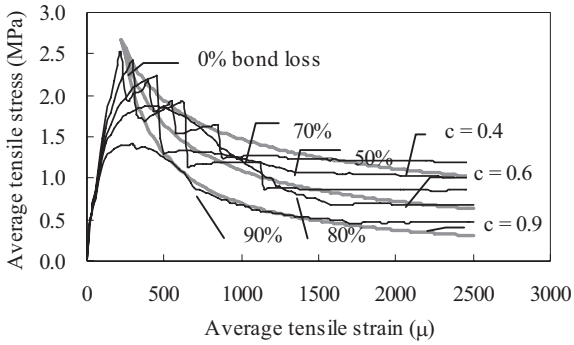

Fig. 29 Average Tensile Stress-Strain Curves (Case1)

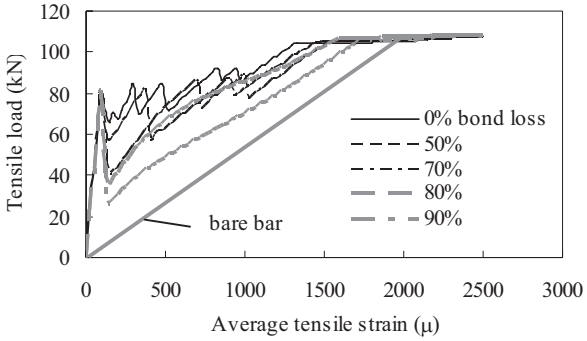

Fig. 30 Tensile Load-Deformation Curves (Case 2)

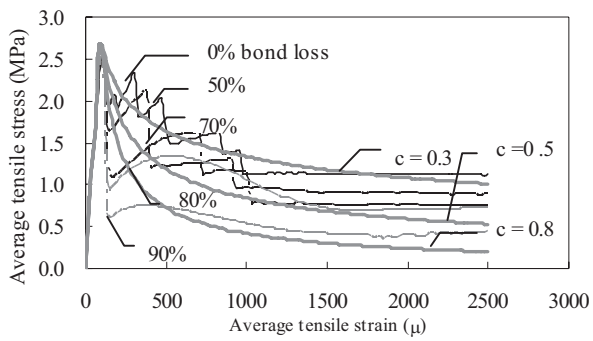

Fig. 31 Average Tensile Stress-Strain Curves (Case2)

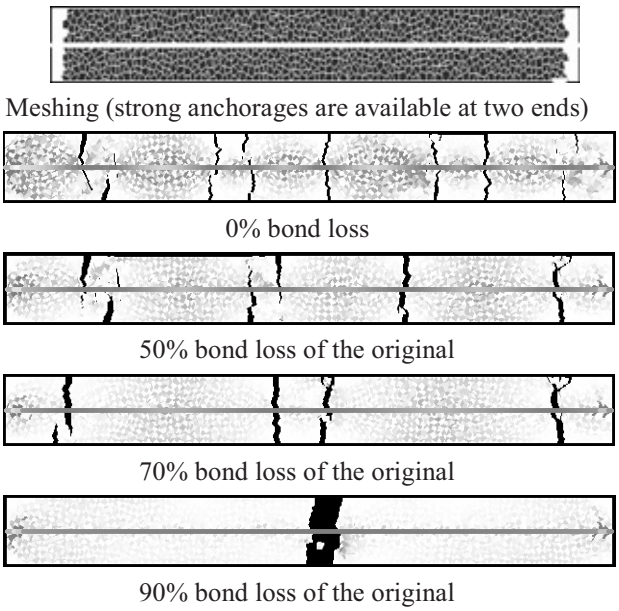

Fig. 32 Crack Distributing Properties Obtained from Analysis in Cases of Good End Anchorages (Case 2)

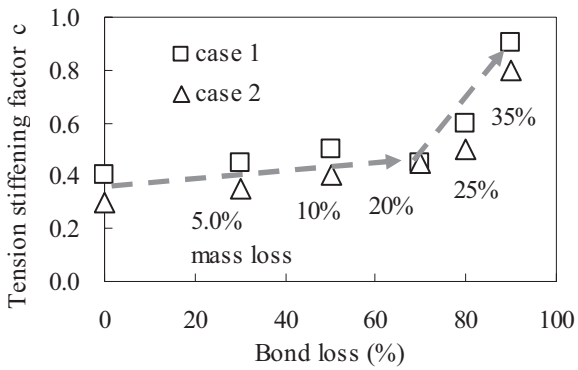

Fig. 33 Tension Stiffening Factor versus Bond-Loss Relationship

of corroded RC members may be no longer a major concern. Hence practically the stiffness degradation in corroded RC members concerning the serviceability may merely depend on the reduction of the steel cross-section and the corrosion induced damages in the concrete cover. The bond loss-induced tension stiffening deterioration may be less influential. In other words, it is inappropriate to link the tension stiffening deterioration solely to the bond loss. Two of them may not be equivalent in the steel corrosion case. Bond focuses more on the local phenomenon while tension stiffening represents more the global response. Other accompanied factors besides the corrosion-induced bond loss like the much increased crack spacing may affect the tension

stiffening in another way. The results from these numerical experimentations can explain the difficulties in clarifying the effect of corrosion-induced bond loss on the tension stiffening factor in the experimental tests as discussed for **Fig. 18.** The main reason is that the corrosion levels applied in the current tests did not cause very severe bond loss.

Once again, it is noticed that, unlike the tension stiffening factor, the localized cracks are always proportionally enlarged with the increase of corrosion level in whichever cases. This is mainly attributed to the increased crack spacing and bond loss. In particular, this localized crack deformation can be more clearly seen in Case 2 study (see **Fig. 32**) since the end slips of each analyzed specimen were prohibited and consequently incorporated into the crack widths within the testing spans in the analysis. Therefore, the localized crack deformation should always be a major concern for the evaluation of the serviceability deterioration of corroded RC members because compared to the tension stiffening loss it is much more sensitive to the corrosion-induced bond loss.

6. Conclusions

Through the extensive experimental and analytical work conducted in this paper, the following conclusions have been drawn up:

(1) The impressed current method shows its applicability to introduce significant un-uniformity of steel corrosion. The normal distribution seems appropriate to describe the un-uniformity. Generally, more severe corrosion corresponds to a greater standard deviation but a smaller coefficient of variation.

(2) The corrosion-induced crack widths at the concrete surface, it-affected loading crack widths, and the localized steel mass losses have good correlations with each other. However, these correlations are weak when the transverse confinement is available. On the other hand, compared to the steel mass loss, the corrosion-induced crack width at the concrete surface seems to be a better parameter for evaluating the bond loss between the corroded steel reinforcement and concrete regardless of the confinement condition.

(3) Increase of steel corrosion level leads to great tension stiffness losses as well as great tension stiffening deterioration of the corroded RC members. Experimental results show that the major factors leading to the stiffness deterioration are the reduction of steel cross-section and the reduction of effective cover concrete. The bond loss-induced tension stiffening deterioration seems not very critical except when the steel corrosion level is extremely high.

(4) Analytical studies show that the changing rates of bond loss and tension stiffening loss with the steel corrosion level are significantly different. Analytically, a steel mass loss at 20% (about 70% bond loss of the original), seems to be a turning point, beyond which the tension stiffening starts to deteriorate rapidly. However, the major concern for corroded RC members beyond this status may be not the serviceability but the safety performance. As a result, in practice analysis of global stiffness degradation of the corroded RC members may need to merely consider the steel loss-induced stiffness loss and the reduction of effective concrete cover.

(5) Both experiments and analysis show that the localized crack deformations should be the major concerns for the structural performance deterioration of corroded RC members related to the serviceability. Moreover, these localized cracks rely intimately on the un-uniformity of steel corrosion.

Acknowledgement

The authors would like to thank Mr M. Watanabe, a current graduate student in Nagaoka University of Technology, for his kind assistance in the experimental work.

References

Amleh, L., and Mirza., S. (1999). “Corrosion Influence on Bond between Steel and Concrete.” *ACI Structural Journal*, .96(3), 415-423.

Amleh, L., and Ghosh, A. (2006). “Modeling the Effect of Corrosion on Bond Strength at the Steel–Concrete Interface with Finite-Element Analysis.” *Can. J. Civ. Eng.*, 33(6), 673-682.

Aramasa, S. (2005). “The Recent Researches on the Effects of Reinforcement Corrosion on Bond Strength between

Reinforcement and Concrete." *Concrete Journal*, Japan Concrete Institute, 43(2), 70-75 (in Japanese).

Auyeung, Y., Balaguru, P., and Chung, L. (2000). "Bond Behavior of Corroded Reinforcement Bars." *ACI Materials Journal*, 97(2), 214-221.

Bolander, J.E and Saito, S. (1998). "Fracture analyses using spring networks with random geometry." *Engineering Fracture Mechanics*, 61(5-6), 569-591.

Bolander, J.E and Le, B.D. (1999). "Modeling crack development in reinforced concrete structures under service loading." *Construction and Building Materials*, 13(1), 23-31.

Comite Euro-International du Beton. 1990. CEB-FIP Model Code, CEB, Paris

Coronelli, D. (2002). "Corrosion Cracking and Bond Strength Modeling for Corroded Bars in Reinforced Concrete." *ACI Structural Journal*, 99(3), 267-276.

Elfgren L., and Noghabai, K. (2002). "Tension of Reinforced Concrete Prisms, Bond Properties of Reinforcement Bars Embedded in Concrete Tie Elements, Summary of a RILEM Round-robin Investigation Arranged by TC 147-FMB'Fracture Mechanics to Anchorage and Bond'", *Materials and Structures*, 35(6), 318-325.

Fang, C., Lundgren, K., Chen, L., and Zhu, C. (2004). "Corrosion Influence on Bond in Reinforced Concrete." *Cement and Concrete Research*, 34(11), 2159-2167.

Japan Concrete Institute, 2004. *Proc. of the Symposium on Long-Term Modeling of Concrete Structures*, JCI-C64.

JSCE, 2006, Performance of Concrete Structures with Material Degradation, *Concrete Engineering Series*, No.71 (in Japanese).

Kawai, T. (1977). "New element models in discrete structural analysis." *Journal of the Society of Naval Architects of Japan*, 141, 174-180 (in Japanese).

Kemp, E. L., and Welhelm, W. J. (1979). "Investigation of the parameters influencing bonding cracking" *ACI Journal, Proceedings*, 76(1), 47-71.

Kato, E., Iwanami, M., Yokota, H., and Ito, H. and Sato, F. (2003). "Bond Behavior between Corroded Rebar and Concrete." *Technical Report of the Port and Airport Research Institute*, No.1044, 17p.

Kato, E., Iwanami, M., Yamaji, T. and Yokota, H. (2006). "Structural Performance and Deterioration due to Chloride Attack of Reinforced Concrete Deck of Existing Piers." *Technical Report of the Port and Airport Research Institute*, No. 1140, 87p.

Nagai, K., Sato, Y. and Ueda, T. (2004). "Mesoscopic Simulation of Failure of Mortar and Concrete by 2D RBSM." *Journal of Advanced Concrete Technology*, 2(3), 359-374.

Nagai, K., Sato, Y. and Ueda, T. (2005). "Mesoscopic Simulation of Failure of Mortar and Concrete by 3D RBSM." *Journal of Advanced Concrete Technology*, 3(2), 385-402.

Lee, H., Noguchi, T., and Tomosawa, F. (2002). "Evaluation of the Bond Properties between Concrete and Reinforcement as a Function of the Degree of Reinforcement Corrosion." *Cement and Concrete Research*, 32, 1313-1318.

Lungren, K. (2005a). "Bond between Ribbed Bars and Concrete. Part 1: Modified model." *Magazine of Concrete Research*, 57(7), 371-382.

Lungren, K., (2005b). "Bond between Ribbed Bars and Concrete. Part 2: "The effect of corrosion." *Magazine of Concrete Research*, 57(7), 383-395.

Matsuo, Y., Okazaki, M, and Shimomura, T. (2001), "Tension Stiffening of RC Members with Rebar Corrosion." *Proceedings of Japan Concrete Institute*, 23(3), 1327-1332.

Nakamura, H, and Higai, T. (1999). "Compressive fracture energy and fracture zone length of concrete." Seminar on post-peak behavior of RC structures subjected to seismic loads, JCI-C51E, 2, 259-272.

Okamura, H., and Maekawa, K. (1991). "Nonlinear analysis and constitutive models of reinforced concrete." Gihido Shuppan.

Okazaki, M., Shimomura, T. and Matsuo, Y. (2003). "Investigation on the Steel Corrosion and Corrosion Cracks Considering of the Non-uniformity Corrosion." *Proceedings of the JCI*, 25(1), 857-862 (in Japanese).

Reinhardt, H.W., Cornelissen H.A.W. and Hordijk D.A. (1986). "Tensile tests and failure analysis of concrete." *Journal of Structural Engineering*, 112(11), 2462-2477.

Saito, S. and Hikosaka, H. (1999). "Numerical analyses of reinforced concrete structures using spring network models", *J. Materials, Cons. Struct. Pavements*, 44(627), 289-303.

Appendix I Distribution of Steel Mass Loss (%)

C_s (%)	Specimen Code												
X (mm)	T1-2	T1-3	T1-4	T1-5	T1-6	T1-C1-2	T1-C2-2	T2-2	T2-3	T2-4	T3-2	T3-3	T3-4
0~100	1.10	2.36	2.86	2.54	9.56	6.29	7.29	0.78	2.21	7.28	0.94	0.58	7.30
100~200	1.24	3.80	3.83	4.56	11.85	13.33	13.07	0.09	1.28	8.64	1.74	0.57	11.32
200~300	1.16	3.98	2.70	5.61	11.65	12.15	9.58	1.38	2.45	11.02	0.82	0.46	12.74
300~400	1.05	2.76	1.54	5.59	11.05	10.90	6.36	0.10	2.04	10.20	0.42	0.27	10.01
400~500	1.04	3.56	1.60	5.81	13.48	8.77	5.41	0.14	2.14	10.54	0.25	1.86	9.94
500~600	0.94	3.20	2.73	4.25	12.34	7.80	10.16	0.75	5.27	9.58	0.80	5.37	13.48
600~700	0.65	3.47	2.71	4.65	10.89	6.86	13.84	2.25	5.15	10.48	2.60	4.10	10.42
700~800	0.52	2.71	1.95	5.46	9.57	6.05	17.11	3.68	4.08	14.41	2.16	3.57	10.56
800~900	0.65	2.90	2.48	4.84	10.37	10.13	12.63	1.95	3.80	11.02	1.17	5.06	10.19
900~1000	0.83	1.67	2.48	6.58	10.03	17.40	7.96	3.08	2.20	15.89	1.92	3.14	9.44
1000~1100	0.04	1.81	2.79	6.60	9.50	19.40	7.94	4.00	2.02	12.60	0.00	3.39	13.78
1100~1200	0.09	2.51	2.98	6.71	9.01	18.01	10.32	3.34	3.72	11.01	1.90	1.93	10.37
1200~1300	0.34	2.86	3.26	5.36	8.90	13.57	17.45	1.45	2.27	11.30	0.93	1.80	12.61
1300~1400	0.31	2.89	2.18	5.71	11.43	13.15	10.72	3.22	3.21	10.30	1.74	2.12	10.45
1400~1500	0.14	2.71	2.17	5.28	15.04	9.15	7.96	1.73	4.35	11.26	1.87	2.42	9.66
1500~1600	0.46	2.44	2.52	5.57	9.94	11.21	10.00	1.99	1.42	8.59	0.17	0.45	11.00
1600~1700	0.55	2.54	2.25	5.31	8.24	14.48	11.06	1.14	2.96	14.00	0.07	0.64	11.41
1700~1800	0.89	2.44	2.10	5.06	7.85	13.41	9.30	1.85	2.04	6.03	1.59	1.28	10.93
1800~1900	1.04	3.08	2.39	6.88	9.72	14.92	15.15	0.00	0.82	8.03	0.29	0.67	8.31
1900~2000	1.71	2.40	2.33	5.04	7.45	10.91	5.75	1.16	0.01	6.35	0.97	0.53	6.75
C_{max} (%)	1.24	3.98	3.83	6.88	15.04	19.40	17.45	4.00	5.27	15.89	2.60	5.37	13.78
C_{min} (%)	0.04	1.67	1.54	4.25	7.85	6.05	5.41	0.00	0.82	6.03	0.00	0.27	8.31
C_{mean} (%)	0.66	2.85	2.48	5.55	10.60	12.26	10.89	1.79	2.84	10.83	1.14	2.17	10.92
S.D	0.38	0.61	0.56	0.76	1.83	3.79	3.42	1.29	1.30	2.37	0.82	1.62	1.44
C.O.V	0.57	0.21	0.22	0.14	0.17	0.31	0.31	0.72	0.46	0.22	0.72	0.74	0.13

Note: X = location of steel reinforcement; C_s = steel mass loss; C_{max} = maximum steel mass loss; C_{min} = minimum steel mass loss; C_{mean} = mean steel mass loss; *S.D* = standard deviation; *and C.O.V* = coefficient of variation.

Appendix II Corrosion-induced Crack Width at the Concrete Surface (mm)

W_{cr} (mm)	Specimen Code												
X (mm)	T1-2	T1-3	T1-4	T1-5	T1-6	T1-C1-2	T1-C2-2	T2-2	T2-3	T2-4	T3-2	T3-3	T3-4
0~100	0.15	0.38	0.25	0.75	0.95	0.50	0.33	0.00	0.40	3.00	0.00	0.00	2.00
100~200	0.18	0.35	0.40	0.85	1.15	0.48	0.38	0.00	0.35	3.00	0.00	0.00	2.00
200~300	0.20	0.30	0.38	0.95	1.35	0.50	0.41	0.00	0.35	3.00	0.00	0.00	2.65
300~400	0.18	0.28	0.40	0.95	1.40	0.50	0.46	0.00	0.40	3.00	0.00	0.00	2.00
400~500	0.18	0.35	0.43	0.90	1.40	0.48	0.48	0.00	0.45	2.50	0.00	0.35	2.00
500~600	0.18	0.40	0.48	0.95	1.45	0.48	0.48	0.00	0.45	2.50	0.15	0.65	2.10
600~700	0.15	0.40	0.53	1.00	1.45	0.53	0.50	0.10	0.50	3.10	0.85	0.65	2.60
700~800	0.15	0.43	0.53	1.00	1.50	0.58	0.55	0.45	0.70	2.05	0.35	0.40	2.05
800~900	0.15	0.43	0.53	0.95	1.55	0.53	0.50	0.15	0.60	2.00	0.15	0.55	1.75
900~1000	0.18	0.37	0.48	0.95	1.35	0.48	0.43	0.20	0.50	2.45	0.45	0.40	2.80
1000~1100	0.18	0.35	0.45	1.00	1.25	0.48	0.43	0.20	0.50	3.05	0.00	0.45	2.65
1100~1200	0.13	0.38	0.50	1.00	1.60	0.48	0.50	0.20	0.55	2.05	0.30	0.15	2.25
1200~1300	0.13	0.38	0.45	0.95	1.65	0.48	0.53	0.15	0.50	2.00	0.15	0.10	2.45
1300~1400	0.15	0.36	0.41	0.90	1.30	0.45	0.50	0.10	0.50	2.00	0.25	0.00	2.15
1400~1500	0.15	0.36	0.43	0.90	1.30	0.40	0.48	0.10	0.35	2.00	0.10	0.25	2.45
1500~1600	0.13	0.33	0.50	0.83	1.30	0.40	0.45	0.00	0.35	4.25	0.05	0.00	2.15
1600~1700	0.10	0.27	0.55	0.73	1.15	0.43	0.40	0.00	0.30	2.05	0.30	0.00	1.70
1700~1800	0.10	0.22	0.53	0.60	1.15	0.42	0.37	0.00	0.20	2.00	0.00	0.00	1.40
1800~1900	0.10	0.20	0.53	0.50	1.25	0.35	0.39	0.00	0.15	1.50	0.00	0.00	2.00
1900~2000	0.10	0.15	0.48	0.45	1.00	0.38	0.37	0.00	0.05	1.50	0.00	0.00	2.00
W_{max} (mm)	0.20	0.43	0.55	1.00	1.65	0.58	0.55	0.45	0.70	4.25	0.85	0.65	2.80
W_{min} (mm)	0.10	0.20	0.38	0.50	1.15	0.35	0.37	0.00	0.15	1.50	0.00	0.00	1.40
W_{mean} (mm)	0.15	0.34	0.47	0.88	1.36	0.47	0.46	0.09	0.43	2.47	0.17	0.22	2.18
S.D	0.03	0.06	0.05	0.14	0.15	0.05	0.05	0.12	0.14	0.66	0.22	0.25	0.37
C.O.V	0.20	0.19	0.12	0.16	0.11	0.12	0.12	1.31	0.32	0.27	1.29	1.12	0.17

Note 1: X = location of steel reinforcement; W_{cr} = corrosion-induced crack widths at the concrete surface; W_{max}, W_{min} = maximum and minimum corrosion-induced crack widths, respectively, at the concrete surface; *S.D* = standard deviation; and *C.O.V* = coefficient of variation.

Note 2: data at the locations of 0~100 mm and 1900~2000 mm were not included in the statistical analysis because half length of the reinforcement segment over there was un-corroded in the experiments.

港湾空港技術研究所報告　第46巻第2号

２００７．６

編集兼発行人　独立行政法人港湾空港技術研究所

発　行　所　独立行政法人港湾空港技術研究所
横須賀市長瀬３丁目１番１号
TEL. 046(844)5040　URL. http://www.pari.go.jp/

印　刷　所　新高速印刷株式会社

CONTENTS